

# ACCURATE WAVENUMBER MEASUREMENT IN HIGH RESOLUTION STIMULATED RAMAN SPECTROSCOPY (SRS) BY USING AN INFRARED STANDARD. $\nu_1$ FUNDAMENTAL OF $^{12}\text{CH}_4$

J. SANTOS, P. CANCIO, J. L. DOMENECH, J. RODRIGUEZ  
and D. BERMEJO

*Instituto de Estructura de la Materia, C.S.I.C., Calle Serrano 119–123,  
Madrid, 28006, Spain*

*(Received 8 August 1991; in final form 15 October 1991)*

A new set of wavenumbers for the Stimulated Raman Spectrum (SRS) of the  $\nu_1$  band of  $^{12}\text{CH}_4$  is presented using the Infrared (IR) absorption spectrum of the  $P_{10}$  component of  $\nu_3$  of the same molecule as a wavenumbers standard. An estimation of the Stark shift due to the pump laser field is experimentally deduced what allows to extrapolate the measured wavenumbers to zero field amplitude. A careful discussion about the main possible error sources and how to cope with them is also included.

The absolute accuracy of the wavenumbers set presented here is believed to be at least one order of magnitude better as compared with previous measurement.

**KEY WORDS:** Molecular Spectroscopy, Laser Spectroscopy.

## 1. INTRODUCTION

Accurate knowledge of molecular energy levels is very important in understanding many processes in different fields, like Combustion, Laser Physics, Astronomy, Chemistry in the atmosphere, etc.

Microwave and infrared (IR) techniques can provide very accurate measurements for the wavenumbers of transitions between vib-rotational levels. Some coherent Raman techniques can provide Doppler limited resolution for many molecules, but the actual precision and accuracy in the determination of wavenumbers is usually poorer as compared with IR techniques of similar resolving power.

The main reason for the higher accuracy provided by the IR spectra may be the availability of many IR absorption standards, measured with different independent procedures, including sub-Doppler techniques. In addition, the very good internal coherence of the Fourier transform techniques make possible the use of standards with relatively low density of spectral lines. Pump and probe techniques, such as Stimulated Raman Scattering (SRS), require the accurate measurement of wavelengths of two independent lasers, usually in the visible region, in order to derive the wavelength of the difference. Very often, good molecular standards can be used to

lock the fixed frequency laser, but the frequency of the tunable laser has to be determined either by means of wavemeters of the Michelson or Fizeau type, or by means of visible standards such as  $I_2$ ,  $Te_2$  or  $NO_2$ , not very accurate as compared with the IR ones. In addition the spectral density of those standards should be very high due to the usually very short continuous scan range (typically  $1\text{ cm}^{-1}$ ) of the lasers.

In our Stimulated Raman/Infrared spectrometer,<sup>1</sup> a fraction of the pump and probe c.w. visible beams can be non-linearly mixed in a  $LiNbO_3$  crystal to generate the IR difference frequency radiation, and the absorption spectrum of an IR standard can be recorded simultaneously with SRS spectrum in order to provide a calibration reference. In this way, it is possible to increase by about one order of magnitude the accuracy of the wavenumbers determined from the SRS spectrum, as compared with most of the above mentioned methods.

A further advantage is that, with visible standards for  $\omega_2$ , the wavenumbers of the probe beam,  $\omega_1$ , has to be accurately known, whereas with IR calibration for  $\omega_1 - \omega_2$  the absolute  $\omega_1$  frequency is of no relevance, as far as its value is kept fixed. Thus, different long term stabilization systems can be used, including stabilized etalons or molecular transitions other than the rather small set that is known at high accuracy level. This enlarges the choice of  $\omega_1$ , and consequently of  $\omega_2$ , and can be very useful in selecting a good combination of dyes for the c.w. ring laser and the pulsed amplifier.

Special care has been put in taking into account the necessary corrections arising from the different data acquisition procedures in the IR and SRS spectra. Also any possible frequency shift in the amplification process of the dye laser (performed for obtaining the SRS spectrum but not for the IR) has been carefully measured and taken into account, as reported in the following paragraphs. The presence of any significant second order Stark effect that could affect the SRS spectrum, has also been checked for the spectrum presented here.

A similar Coherent Raman/IR spectrometer has been reported previously,<sup>2</sup> the main difference being that CARS technique was used instead of SRS.

The totally symmetric  $\nu_1$  band of  $^{12}CH_4$ , is inactive in the IR spectrum but has a very high Raman scattering cross section.<sup>3</sup> For that reason the high resolution SRS and CARS spectra of this band are among the first spectra reported by this technique.<sup>4</sup> Later on, some other measurements have been reported,<sup>5-8</sup> along with several semi-empirical fits of the experimental data.<sup>9,10</sup> Our initial interest in this study was to check the accuracy of our Raman/IR spectrometer. However, quite surprisingly, we found that no accurate unambiguous set of wavenumbers existed for this band. We report here a wavenumbers set for all the resolved peaks observed in the 77 K SRS spectrum, increasing the accuracy by more than one order of magnitude as compared with most of the previously reported values.

The remainder of the paper is organized as follows: part 2 presents a description of the apparatus, paying special attention to the acquisition system, part 3 is a discussion of the frequency calibration system used and part 4 presents a comparison with previous experimental and theoretical work.

## 2. EXPERIMENTAL

The IR and Raman Laser Spectrometers have been described elsewhere<sup>1,11</sup> for what we shall focus our description here to some aspects relevant to the calibration of Raman frequencies against infrared standards.

The apparatus is depicted in Figure 1. The IR radiation is generated in a  $\text{LiNbO}_3$  crystal by non-linear mixing of the emission of a single-mode  $\text{Ar}^+$  laser, at fixed frequency  $\omega_1$ , with that of a tunable single-mode ring dye laser,  $\omega_2$ . Phase matching for crossed polarizations with collinear beams is obtained by tuning the temperature of the crystal.<sup>12,13</sup> Its spectral bandwidth is determined by that of the visible lasers. In our case, is of 2 MHz ( $0.7 \times 10^{-4} \text{ cm}^{-1}$ ).

Either the dye or both dye and  $\text{Ar}^+$  lasers are amplitude modulated and lock-in amplifiers are used for detecting the IR signal.

For the stimulated Raman Spectrometer, a quasi-c.w. configuration has been chosen,<sup>14,15</sup> sharing the same two visible lasers used for generating the IR radiation. The c.w. emission of the  $\text{Ar}^+$  laser is mechanically chopped in order to obtain 80  $\mu\text{s}$  pulses and used as probe beam. The pump beam is obtained by pulse amplifying the emission of the c.w. laser in a three-stages dye amplifier pumped by an injection seeded single-mode Nd-YAG laser. After mixing in a dichroic mirror the two collinear beams are focussed on the sample using a  $F = 50 \text{ cm}$  lens. The diameter of the probe beam is matched to that of the pump beam ( $D = \pi\omega = 8 \text{ mm}$ ,  $\omega$  being the Gaussian spot size). The spot diameter at the focus is  $D_0 \approx 100 \mu\text{m}$ .

For  $\omega_1 - \omega_2 = \omega_R$ , corresponding to a Raman allowed transition in the sample, a small absorption ( $\omega_1 > \omega_2$ , Inverse Raman) or amplification ( $\omega_1 < \omega_2$ , Raman gain) is produced in the probe beam, in the time scale of the pump beam (12 ns FWHM). This signal is acquired by means of a boxcar averager. The instrumental resolution is limited in this case by the Fourier transform of the temporal pulse shape of the pump beam, which corresponds to a Gaussian profile with FWHM = 60 MHz ( $\sim 2 \times 10^{-3} \text{ cm}^{-1}$ ).

Several effects can make this resolution limit difficult to achieve. First, if the YAG laser is not single-mode, the beating between different modes is transferred in some extension to the temporal profile of the pump beam, which originates a non-Gaussian

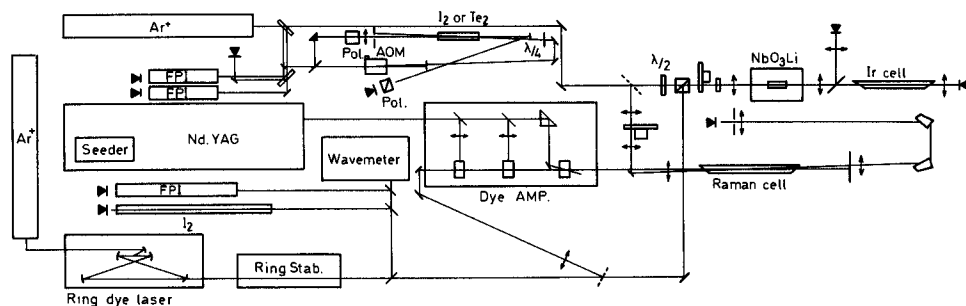


**Figure 1** Schematic diagram of the Raman/IR Spectrometer (FPI: Fabry-Perot Confocal Interferometer).

spectral lineshape with sidebands, leading to some distortion in the spectrum. Second, the high power density at the focal region interacts with the energy levels of the molecule through the AC-Stark effect, giving rise to line broadening and shift. The influence of this effect on the methane spectrum reported here will be discussed later on.

In order to record Raman and IR spectra simultaneously, a small fraction of the c.w. Ar<sup>+</sup> and dye lasers is pick off before entering the Raman system, and used to generate the IR radiation.

Two sets of spectra were recorded (Figure 3). The first one with a sample pressure of 15 Torr at room temperature. This spectrum is essentially Doppler limited but several lines are unresolved. A second set was recorded cooling the cell in a liquid nitrogen bath at 77 K, at the vapor pressure of 10 Torr. The spectrum appears almost fully resolved and the S/N ratio is well over 1000. The pump energy was set to 10 mJ. The good S/N ratio allowed us to record several spectra at low pump energy (1 mJ) and still very good S/N (over 200) in order to check for a Stark shift in the Raman frequencies.

### 2.1 Data Acquisition System

The data acquisition is controlled by a microcomputer, which commands the beginning of the dye laser scan and acquires data from several channels in a microprocessor based A/D converter.

In order to account for the non-linearity of the dye laser scan, the transmission fringes of a confocal temperature stabilized Fabry-Perot (FP) interferometer of 150 MHz free spectral range (FSR) and Finesse  $\approx 200$  are recorded. An electronic system (Figure 2), has been devised in order to avoid the need of storing the great number of data points required to sample the very sharp (1 MHz) transmission peaks of the FP etalon.

The shots from the YAG laser are used as the main clock for the acquisition system. Averaged data points from the Raman signal are acquired every several shots. The IR signal from the lock-in amplifier is sampled at the same rate.

The output of the FP is continuously monitored as the frequency is scanned. Each time  $\omega_2 = m \times \text{FSR}$  ( $m$  integer) a sharp peak appears in the photodiode output, and the derivative of this signal triggers a counter. Once triggered, each YAG shot increases its output by one step. At every data acquisition, this output is read, its value being zero if no etalon mark has appeared since the last reading or a nonzero value proportional to the time elapsed since the etalon mark appeared and the counter is reset to zero by the next clock pulse. The actual position of the frequency mark is recovered by the data analysis software.

By choosing the number of data points per wavenumber and the number of shots to be averaged, we can select the precision of the frequency marks, which is usually chosen to be of the same order of the laser frequency jitter (in the range of  $0.3\text{--}1.0 \times 10^{-4} \text{ cm}^{-1}$ ).

Two experimental effects need to be taken into account when comparing the Raman spectrum with the IR one. The first one is due to the different data acquisition system in the IR and Raman spectra. Each IR data point reflects the intensity at the current

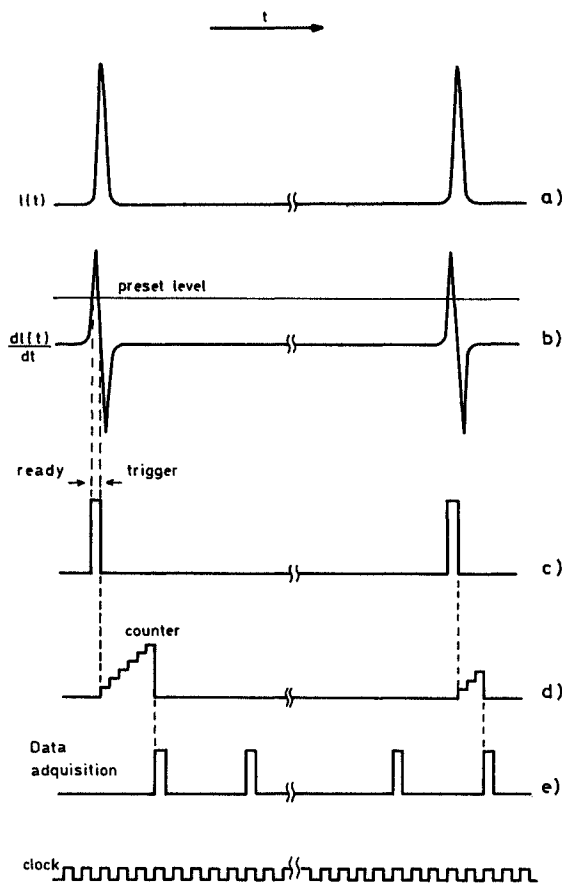


**Figure 2** Timing sequence of the frequency marks acquisition system. The time derivative of the transmission of a temperature stabilized confocal FP interferometer, (a), is compared with a preset level, (b), and triggers, (c), a counter, (d), whose output is read at the same rate as Raman and IR channels, (e), allowing the retrieval of the peak actual time position.

wavenumber, whereas the Raman signal at the same instant is an average of several previous shots, each for a different wavenumber because the dye laser is continuously scanned. This originates an apparent shift in the wavenumber of the Raman peak, whose value depends on the number of averaged points and on the scan rate. Second, the wavenumber of the IR radiation, depends on that of the c.w. dye laser, whereas the Raman signal is actually generated by the pulse amplified laser. A small frequency shift can occur in the amplification process. The magnitude and sign of this shift depends upon the dye used for amplification and the spectral region involved.

The correction needed to cope with both effects is obtained (see Ref. 11 for details) from a comparison of the peak positions in the visible  $I_2$  absorption spectra recorded simultaneously by using the c.w. and pulse amplified dye lasers.

### 3. WAVENUMBERS CALIBRATION

The frequency of the Ar<sup>+</sup> laser,  $\omega_1$ , is locked to a hyperfine transition of  $^{127}\text{I}_2$  using a polarization spectroscopy technique.<sup>16</sup> Taking into account both jitter and long term drift of the servolock we can estimate the absolute accuracy of  $\omega_1$  to be better than 1 MHz.

The FSR of the etalon has been carefully measured by recording the IR spectra of different standards ( $\text{CH}_4$ ,<sup>17</sup>  $\text{N}_2\text{O}$ <sup>18</sup>), for different choices of  $\omega_1$ , in order to cover the whole working range of the dye laser,  $\omega_2$  (16.000–17.700  $\text{cm}^{-1}$ ) needed for a full coverage of relevant vibrational regions. No significant variation in the FSR has been detected in this region. The precision of relative frequency measurements is  $10^{-4}\Delta\omega$ , what allows for errors lower than  $10^{-4}\text{cm}^{-1}$  within each 1  $\text{cm}^{-1}$  continuous scan.

In early work, or for the spectral regions where IR cannot be generated, a reference spectrum of the absorption of the dye laser by a  $^{127}\text{I}_2$  cell was recorded simultaneously with the Raman spectrum. The  $^{127}\text{I}_2$  visible absorption spectrum<sup>19</sup> has a very high density of lines, with a fairly homogeneous coverage of the spectral regions of interest for  $\omega_2$ . The claimed accuracy is  $2 \times 10^{-3}\text{cm}^{-1}$  for isolated, intense lines. This figure is too high to take full advantage of our high resolution capabilities.

In the joint Raman-IR configuration reported here we can take advantage of the lower (linear with frequency) Doppler limit in the IR region and the usually lower spectral congestion of vib-rotational spectra as compared to rovibronic existing absorption standards.

For the present Raman study of the  $\nu_1$  Q-branch, we have chosen the  $\text{CH}_4$   $\nu_3$  P<sub>10</sub> sub-branch as IR reference. These transitions are Raman allowed as well, but they are far too weak to be observed in our Raman spectrum.

The accuracy of the reported IR line wavenumbers is  $5 \times 10^{-4}\text{cm}^{-1}$  (twice the standard error), as compared to  $2 \times 10^{-3}\text{cm}^{-1}$  for the  $\text{I}_2$ .

The different error sources from the several steps leading to relative frequency calibration are routinely estimated in the data analysis software, using standard methods. This estimated error is listed in *Table 1* along with the wavenumbers and represents the contribution of the dye laser jitter and noise, as well as that of the width and blending of the lines. A typical figure for unblended lines in our spectrum is  $3 \times 10^{-4}\text{cm}^{-1}$  (s.d.), and is coincident with the standard deviation actually found for the wavenumbers of the same transitions in ten different records.

Besides this reproducibility figure, we must consider the error estimated for the correction applied to Raman wavenumbers (see previous paragraph), and the error quoted for the reference spectrum. The overall uncertainty in the wavenumbers reported in *Table 1* is estimated to be  $1 \times 10^{-3}\text{cm}^{-1}$  (twice s.d.).

#### 3.1 Stark Effect

As mentioned above, the molecular energy levels are perturbed by the electromagnetic radiation field. Even for non-polar molecules the strong field due to the pump beam interacts with the induced dipole moment, originating an energy shift proportional to the instantaneous intensity.<sup>20,21</sup> The major manifestations of this AC-Stark effect are a small change in the inertial moments, the removal of the  $M$  degeneracy and a

global vibrational energy shift, which is proportional to the derivative of the molecular polarizability respect to the normal coordinates.

The  $|M|$  splitting and  $J$ -dependent shift is only very slowly dependent on the vibrational quantum numbers and for  $\Delta J = 0$ ,  $\Delta M = 0$  transitions, no splitting is observable in vibrational  $Q$ -branches.<sup>21,22</sup> Nevertheless, the power-dependent vibrational shift can give rise to an inhomogeneous broadening as the field amplitude varies in time and is different for different regions in the sample contributing to the Raman signal.

Theoretical calculations for diatomic molecules<sup>20,21</sup> show that the vibrational energy shift is linearly dependent on the derivative of the molecular polarizability with respect to the normal coordinate,  $\partial\alpha/\partial Q$ , and of opposite sign.

We have measured the Stark shift for the methane  $\nu_1$  band by comparing the peak positions at two energy levels (10 mJ and 1 mJ) corresponding to peak intensities of  $\sim 50 \text{ GW/cm}^2$  and  $\sim 5 \text{ GW/cm}^2$  for the peak of the gaussian distribution at the focal plane. We found a value of  $-0.5 \times 10^{-4} \text{ cm}^{-1}/\text{mJ}$ .

The lines are 10% broader in the high pump power spectrum. In the low power one, the Gaussian FWHM is  $6.3 \pm 0.5 \times 10^{-3} \text{ cm}^{-1}$ , close to the value of  $5.2 \times 10^{-3} \text{ cm}^{-1}$  expected from the convolution of the Doppler ( $4.6 \times 10^{-3} \text{ cm}^{-1}$ , at 77 K) and instrumental ( $2.3 \times 10^{-3} \text{ cm}^{-1}$ ) linewidths.

The wavenumbers in *Table 1* have been extrapolated to zero field amplitude by adding  $5 \times 10^{-4} \text{ cm}^{-1}$  to the values of the 10 mJ spectrum.

#### 4. RESULTS AND DISCUSSION

Figure 3 shows the 77 K spectrum of the  $\nu_1$  band of  $\text{CH}_4$  (lower field), together with the IR spectrum of the  $\nu_3, P_{10}$  sub-branch of the same molecule used as reference.

*Table 1* summarizes the line positions for  $J \leq 11$  of the  $\nu_1$  band of  $^{12}\text{CH}_4$ , calculated and measured by different Raman techniques. The accuracy claimed by their authors is also reported. The first column list the most probable assignment following the notation first introduced by Moret-Bailly.<sup>23</sup> Columns under the heads, "Owyong", "Lavorel" and "Present work", list SRS data. Owyong data correspond to c.w. operation for what no relevant Stark shift is expected. This effect should be present in the Lavorel data, but to our knowledge, no attempt was done to correct for this fact. Consequently, wavenumbers in this column could be slightly red-shifted. A  $0.006 \text{ cm}^{-1}$  calibration error has been suggested in Ref. 9 for the Owyong data. It should be noticed that adding  $0.006 \text{ cm}^{-1}$  to all the Owyong wavenumbers, bring them into much better agreement with most of the other wavenumbers listed in *Table 1*.

The column under the head "Kozlov" correspond to c.w. CARS data from Ref. 5, where the best resolved spectrum up to date is reported. Only relative peak positions are listed. An appreciable discrepancy with most of the other available data is observed increasing with increasing wavenumbers.

The "Schrötter" column, corresponds to an empirical fit including the c.w. CARS data from Refs. 6 and 24 together with other experimental data previously published or known by private communications.

Table 1 Observed and calculated wavenumbers in the  $\nu_1$  Raman band of  $^{12}\text{CH}_4$  ( $\text{cm}^{-1}$ )

Assignment <sup>(a)</sup>	Owong <sup>(b)</sup>	Graener <sup>(c)</sup>	Kozlov <sup>(d)</sup>	Schrüfer <sup>(e)</sup> (emp. fit)	Lavorel <sup>(f)</sup>	Lolck <sup>(g)</sup> (calculated)	Present work <sup>(h)</sup>	Relative peak height <sup>(h)</sup>	
								77 K	295 K
J = 0 A <sub>1</sub> (0)	2916.472			2916.478	2916.479	2916.4885	2916.4812 (3)	420	81
J = 1 F <sub>1</sub> (0)	.4935	.5021	.4989	.499	.500	.5083	.5023 (3)	624	170
J = 2 E(0)	.5335	.5416	.5340	.538	.541	.5457	.5433 (3)	1000	500
J = 2 F <sub>2</sub> (0)		.5450							
J = 3 F <sub>1</sub> (0)	.6065	.5945	.5793	.590	.600	.6042	.5952 (4)	575	424
J = 3 F <sub>2</sub> (0)		.6035	.5888	.600	.6035 (4)	.589			
J = 3 A <sub>2</sub> (0)		.6162	.5979	.5979	.612	.6152	.6157 (3)	.615	615
J = 10 A <sub>2</sub> (0)				.640		.6348			
J = 4 A <sub>1</sub> (0)	.635		.6220	.641		.6423	.6438 (3)	584	863
J = 4 F <sub>1</sub> (0)	.650		.6363	.656		.6565	.6591 (3)	332	
J = 10 F <sub>2</sub> (2)				.663		.6567		222	410
J = 4 E(0)	.661		.6440	.668		.6667	.6696 (4)		
J = 9 F <sub>2</sub> (0)				.675		.6680		507	1000
J = 5 F <sub>1</sub> (0)	.695		.6757	.701		.6953	.7031 (3)		
J = 4 F <sub>2</sub> (0)				.700		.6990		126	473
J = 9 F <sub>1</sub> (0)				.704		.7014			
J = 5 F <sub>2</sub> (0)				.725		.7222	.7275 (3)	41	791
J = 8 A <sub>1</sub> (0)	.736		.6992	.738		.7346	.7408 (10)		
J = 6 E(0)				.739		.7356		55	686
J = 8 F <sub>1</sub> (1)				.744		.7412			
J = 6 F <sub>2</sub> (1)				.748		.7444		84	274
J = 7 F <sub>1</sub> (0)				.748		.7451			
J = 6 F <sub>2</sub> (0)	.767		.7459	.775		.7507	.7508 (5)	98	338
J = 5 E(0)	.796			.770		.7664			
J = 5 F <sub>1</sub> (1)	.8075			.802		.7954	.7779 (4)	124	686
J = 5 F <sub>2</sub> (0)				.813		.8076	.8036 (4)		
J = 1 F <sub>1</sub> (1)							.8162 (4)		



J = 6	$F_2(0)$	.904	.910	.9031	.9140 (3)	41	275
	$F_1(0)$	.935	.940	.9329	.9451 (5)	41	291
	$A_1(0)$	.965	.968	.9602	.9727 (3)	86	497
J = 7	$A_2(0)$	.9825	.988	.9812	.9917 (3)	16	390
	$F_2(1)$	2917.034	2917.038	2917.0308	2917.0423 (3)	8	216
	$E(0)$	.064	.670	.0610	.730 (3)	5	145
J = 8	$F_2(1)$	.120	.128	.1160	.1313 (3)	8	344
J = 7	$F_1(1)$	.178	.186	.1182	.1854 (3)	2	147
J = 8	$F_1(0)$	.263	.261	.1768	.2717 (7)	2	100
J = 9	$E(0)$	.287	.295	.2559	.2946 (3)	2	341
J = 8	$E(0)$	.3095	.296	.2844	.3173 (3)	2	160
J = 9	$A_1(0)$	.392	.318	.2947	.4000 (6)	61	61
J = 8	$F_2(0)$	.431	.398	.3071	.4386 (6)	65	65
J = 10	$F_1(1)$	.464		.4053	.4709	111	111
J = 9	$F_1(2)$	.503			.5095 (3)	8	108
J = 10	$F_2(1)$	.538			.5454 (6)	188	188
J = 11	$F_2(1)$	.612			.6210 (10)	31	31
J = 10	$F_1(0)$	.676			.6764 (3)	203	203
J = 10	$A_1(0)$	.686			.6933 (4)	51	51
J = 10	$E(0)$	.755			.7310 (10)	8	8
J = 11	$F_2(0)$	.767			.7623 (10)	77	77
J = 11	$A_2(0)$				.7732 (10)	76	76

<sup>(a)</sup> Following the notation introduced by Moret-Bailly.<sup>2,3</sup>  
<sup>(b)</sup> SRS data. Reference 4. Absolute accuracy: .01  $\text{cm}^{-1}$ . Relative positions of the stronger lines < .001  $\text{cm}^{-1}$  (s.d.). An overall calibration correction of + .006  $\text{cm}^{-1}$  has been suggested in Ref. 9.  
<sup>(c)</sup> FT data. Evaluated by adding 2916.4812 to the relative positions reported in Ref. 7. Accuracy of the relative positions between 2 and  $15 \times 10^{-4} \text{cm}^{-1}$ .  
<sup>(d)</sup> CARS data. Evaluated by adding 2916.4812 to the relative positions reported in Ref. 5. Absolute precision of .01  $\text{cm}^{-1}$ .  
<sup>(e)</sup> Empirical fit. Reference 6. and 14. Absolute accuracy, .02  $\text{cm}^{-1}$ . Relative positions accuracy, .005  $\text{cm}^{-1}$ .  
<sup>(f)</sup> SRS data. Reference 8. Absolute precision of .001  $\text{cm}^{-1}$ .  
<sup>(g)</sup> Reference 1.  
<sup>(h)</sup> SRS data. In parenthesis, estimated relative accuracy in units of  $10^{-4} \text{cm}^{-1}$  (s.d.). Absolute accuracy, .0005  $\text{cm}^{-1}$  (s.d.).  
<sup>(i)</sup> Present work, relative to the strongest peak given as 100.

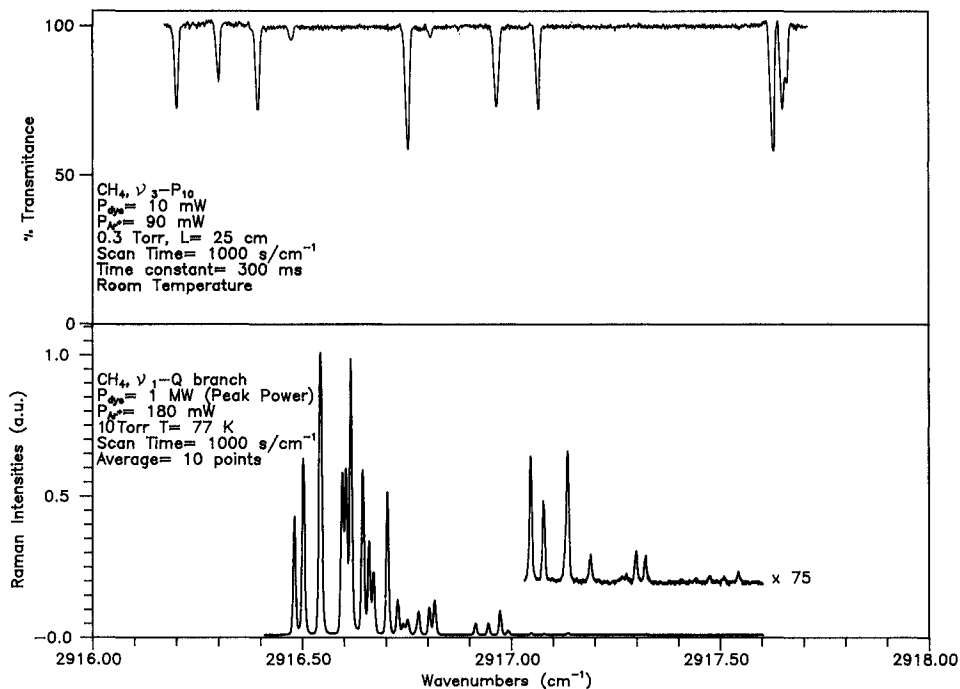


**Figure 3**  $\text{CH}_4$   $\nu_1$   $Q$ -branch Stimulated Raman Spectrum at 77 K (lower field) and  $\nu_3$   $P_{10}$  IR reference spectrum used for calibration (upper field).

The “Graener” column has been deduced by adding 2916.4812 to the relative line positions of Ref. 7, obtained by FT-Raman.

The column headed “Lolck” reports a wavenumber prediction based on molecular constants deduced from experimental data from Ref. 9 and other infrared data.

Under the head “Present work”, our pulsed SRS experimental wavenumbers are reported. The estimated relative uncertainties in units of  $10^{-4} \text{ cm}^{-1}$  are indicated in parenthesis. After applying the experimental corrections discussed above, a  $+0.0005 \text{ cm}^{-1}$  correction has been done to refer the measured wavenumbers to zero field amplitude. They reflect the average of between five and twelve independent measurements, using the IR spectrum as a standard, in the way described above. The absolute accuracy for this data set is estimated to be at least one order of magnitude better than previously published data.

### Acknowledgements

This work has been carried out under the Research Project PB89-0041, financed by the Spanish DGICYT.

### References

1. D. Bermejo, J. L. Domenech, P. Cancio, J. Santos and R. Escribano, in “Laser Spectroscopy IX”, Academic Press, Inc., M. S. Feld, J. E. Thomas and A. Mooradian (eds.), p. 126 (1989).

2. S. Yu. Volkov, D. N. Kozlov, P. V. Nikles, *et al.*, *Kvantovaya Elektron.* **8**, 223 (1981).
3. D. Bermejo, R. Escribano and J. M. Orza, *J. Mol. Spectrosc.* **6**, 345 (1977).
4. A. Owyong, C. W. Patterson and R. S. McDowell, *Chem. Phys. Lett.* **59**, 156 (1978).
5. D. N. Kozlov, A. M. Prokhorov and V. Smirnov, *J. Mol. Spectrosc.* **77**, 21 (1979).
6. H. Frunder, D. Illiq, H. Finsterhölzl, W. H. Schrötter, B. Lavorel, G. Roussel, J. C. Hillico, J. P. Champion, G. Pierre, G. Poussigue and E. Pascaud, *Chem. Phys. Lett.* **106** (1983).
7. M. Graener and A. Laubereau, *Optic. Comm.* **54**, 141 (1985).
8. B. Lovorel and M. Terki-Hassaine, personal communication, reported in ref. 24
9. J. E. Lolck, A. G. Robiette and L. R. Brown, *J. Mol. Spectrosc.* **92**, 229 (1982).
10. J. E. Lolck, *Chem. Phys. Lett.* **106**, 143 (1984).
11. D. Bermejo, J. Santos, P. Cancio, J. L. Domenech, C. Domingo, J. M. Orza, J. Ortigoso, and R. Escribano, *J. Raman Spectrosc.* **21**, 197 (1990).
12. H. Fay, W. J. Alford and H. M. Dess, *Appl. Phys. Lett.* **12**, 89 (1968).
13. A. S. Pine, *J. Opt. Soc. Am.*, **64**, 1683 (1974).
14. A. Owyong, in "Laser Spectroscopy", Vol. IV, H. Walther and K. W. Rothe (eds.), Springer, Berlin, p. 175 (1979).
15. P. Esherick and A. Owyong, in "Advances in Infrared and Raman Spectroscopy", Vol. 9, R. J. H. Clark and R. E. Hester (eds.), Heyden Ltd., p. 130 (1982).
16. M. Raab and A. Weber, *J. Opt. Soc. Am.* **2**, 1476 (1985).
17. A. S. Pine, *J. Opt. Soc. Am.* **66**, 97 (1976).
18. G. Guelachvili and K. N. Rao, "Handbook of Infrared Standards", Academic Press, Inc. (1986).
19. S. Gerstenkorn and P. Luc, "Atlas du Spectre d'Asorption de la Molécule d'iode", CNRS, Paris (1978).
20. L. A. Rahn, R. L. Farrow, M. L. Koszykowski and P. L. Mattern, *Phys. Rev. Lett.* **45**, 620 (1980).
21. M. Péalat, M. Lefebvre, J. P. E. Taran and P. L. Kelley, *Phys. Rev.* **A38**, 1948 (1988).
22. J. W. Nibler, in "Applied Laser Spectroscopy", W. Demtröder and M. Inguscio (eds.), Plenum Press, N. York, p. 313–328 (1990).
23. M. Moret-Bailly, *Cah. Phys.* **15**, 237 (1961).
24. H. W. Schrötter, H. Frunder, H. Berger, J.-P. Boquillon and G. Millot, in "Advances in Non-linear spectroscopy", R. J. H. Clark and R. E. Hester (eds.), John Wiley Ltd., p. 97 (1988).